# Consistent optical potential for incident and emitted low-energy $\alpha$ particles

V. Avrigeanu* and M. Avrigeanu
*Horia Hulubei National Institute for Physics and Nuclear Engineering, P.O. Box MG-6, 077125 Bucharest-Magurele, Romania*
(Received 25 March 2015; revised manuscript received 20 May 2015; published 17 June 2015)

Recent measurements of $\alpha$-particle induced reactions on the $^{64}$Zn nucleus, below and around the Coulomb barrier, are analyzed simultaneously with $\alpha$-particle emission at similar energies in proton-induced reactions on Zn isotopes. All open reaction channels, particularly the $\gamma$ decay, are calculated using consistent input parameters. Additionally, we check a previous optical-model potential for $\alpha$ particles on nuclei within the mass number range $45 \leqslant A \leqslant 209$ [Avrigeanu *et al.*, Phys. Rev. C **90**, 044612 (2014)] and prove its correctness in the outgoing channel at least for the present case involving $^{64}$Zn and nearby nuclei. The reliability of this potential for incident as well as emitted low-energy $\alpha$ particles is supported by the successful reproduction of high-precision measured data, using no empirical rescaling factor of the $\gamma$ and/or particle widths.

DOI: 10.1103/PhysRevC.91.064611 PACS number(s): 24.10.Ht, 24.60.Dr, 25.55.−e, 27.50.+e

## I. INTRODUCTION

Newly published proton-induced reaction cross sections for $\alpha$-particle emission at energies below and around the Coulomb barrier $B$ [1] offer the opportunity to study the related optical model potential (OMP) on far better terms than ever before. Actually, the analysis of $\alpha$-emission cross sections within the statistical model (SM) should first concern excitation energies lower than 15–20 MeV, in order to avoid additional pre-equilibrium emission (PE) effects. Even so, the calculated cross sections would still heavily depend on residual nucleus level density and competitive emission of $\gamma$ rays and nucleons. The level-density effects could be also avoided by limiting of the incident energy so that low-lying discrete levels are mainly fed by the emitted $\alpha$ particles [2]. However, the competition of $\gamma$-ray and nucleon emission may still have a strong effect on the calculated cross sections. This is why $(p,\alpha)$ reaction data for the target nucleus $^{64}$Zn, at energies even below the $(p,n)$ reaction threshold, have been proven to be most useful for the study of the $\alpha$-particle OMP [1]. As a result, these data have been used for further work on an $\alpha$-particle OMP for nuclei within the mass number range $45 \leqslant A \leqslant 209$ [3].

Previous attempts in this area pointed out a significant underestimation of the $\alpha$-particle emission [2,4] by OMPs established through the analysis of the $\alpha$-particle elastic scattering, obviously above $B$ [5,6]. These works have not taken into account the particular $\alpha$-particle nuclear surface absorption below $B$, with a specific energy dependence of the surface imaginary potential depth [3,7,8] validated by description of the $\alpha$-induced reaction data at lower incident energies. Since this energy range is also related to the $\alpha$-particle emission just above the effective thresholds of various nucleon-induced reactions, we may have now different expectations concerning the proper account of the emitted $\alpha$ particles. Additionally, we also test the OMP [3] using recent and accurate $(\alpha,x)$ reaction data [9] for the same $^{64}$Zn target nucleus, below and around $B$.

A reliable SM analysis of high-precision reaction data should concern the available data for all reaction channels as well as the different isotopes of the same element. It should also use consistent input model parameters established or validated by means of various independent data analysis. The $\gamma$-ray strength functions are the most important among them, while the $\gamma$-ray competition account is critical for a suitable description of $\alpha$-induced reactions well below $B$, and thus for the final $\alpha$-particle OMP assessment. At the same time, the description of both $\gamma$-ray and $\alpha$-particle emission have been proven problematic in the case of the above-mentioned study of protons on $^{64}$Zn [1], especially within global model calculations. Therefore we analyze the similar data for all isotopes $^{64,66-68,70}$Zn in order to support the OMP for emitted $\alpha$ particles.

The consistent SM parameters involved in the present model calculations have formerly been derived from independent data. They are discussed in Sec. II, which includes the results for the $(p,n)$ and $(p,\gamma)$ reactions on Zn isotopes, used for the validation of the proton and $\gamma$-ray transmission coefficients, respectively. The results corresponding to the OMP of Ref. [3] are then compared with the measured cross sections of $(\alpha,x)$ reaction on $^{64}$Zn [9] and $(p,\alpha)$ reactions on Zn isotopes in Sec. III, followed by conclusions in Sec. IV.

## II. NUCLEAR MODEL PARAMETERS

The $(\alpha,x)$ and $(p,\alpha)$ reaction analysis carried out in this work made use of a consistent set of nucleon and $\gamma$-ray transmission coefficients, and back-shifted Fermi gas (BSFG) nuclear level densities [10]. Their parameters were established or validated on the basis of independent experimental information for neutron total cross sections $\sigma_T$ and $(p,n)$ reaction cross sections [11], $\gamma$-ray strength functions of Cu, Zn, and Ga isotopes, and low-lying levels [12] and neutron resonance data [13] (columns 4–9 of Table I), respectively. Hereafter only the points in addition to the details given formerly [3,7,8] are mentioned as well as the particular parameter values that could be used within further trials.

The PE and compound-nucleus (CN) model calculations discussed in the following were carried out within a local approach using an updated version of the computer code STAPRE-H95 [14], while there are also shown the default predictions of the well-known TALYS code [15] in order to

*vlad.avrigeanu@nipne.ro

 

TABLE I. Low-lying levels number $N_d$ up to excitation energy $E_d^*$ [12] used in cross-section SM calculations, the low-lying levels and $s$-wave nucleon-resonance spacings $D_0^{\rm exp}$ (with uncertainties given in parentheses, in units of the last digit) in the energy range $\Delta E$ above the separation energy $S$, for the target-nucleus ground state (g.s.) spin $I_0$, fitted to obtain the BSFG level-density parameter $a$ and g.s. shift $\Delta$ (for a spin cutoff factor calculated with a variable moment of inertia [17] between half and 75% of the rigid-body value, from g.s. to $S$, and reduced radius $r_0 = 1.25$ fm), and the average radiation widths $\Gamma_\gamma$, either measured [13] or based on systematics (given between square brackets), and corresponding to the EGLO model parameter $T_f = 0.5$ MeV used for description of the RSF data [28,31].

| Nucleus | $N_d$ | $E_d^*$ | Fitted low-lying levels and nucleon-resonance data | | | | | | $a$ | $\Delta$ | $\Gamma_\gamma$ |
|---|---|---|---|---|---|---|---|---|---|---|---|
| | | (MeV) | $N_d$ | $E_d^*$ (MeV) | $S+\frac{\Delta E}{2}$ (MeV) | $I_0$ | $D_0^{\rm exp}$ (keV) | $\Gamma_\gamma$ (meV) | (MeV$^{-1}$) | (MeV) | (meV) |
| $^{61}$Cu | 36 | 3.092 | 32 | 3.019 | | | | | 6.55 | –0.67 | |
| $^{63}$Cu | 60 | 3.291 | 79 | 3.565 | 9.026 | 0 | 5.9(7)[a] | | 6.81 | –0.85 | |
| $^{64}$Cu | 40 | 1.780 | 40 | 1.780 | 7.993 | 3/2 | 0.70(9)[b] | 490(30) | 7.70 | –1.55 | |
| $^{64}$Zn | 41 | 3.628 | 49 | 3.795 | | | | | 7.00 | –0.03 | |
| $^{64}$Ga | 17 | 0.852 | 17 | 0.852 | | | | | 7.45 | –2.10 | |
| $^{65}$Cu | 48 | 3.278 | 48 | 3.278 | | | | | 7.85 | –0.10 | |
| $^{65}$Zn | 31 | 2.216 | 31 | 2.216 | 8.018 | 0 | 2.3(3)[b] | 726(60) | 8.40 | –0.60 | |
| $^{65}$Ga | 25 | 2.046 | 25 | 2.046 | 11.896 | | | [510(200)] | 8.00 | –0.75 | 960 |
| $^{66}$Cu | 22 | 1.439 | 22 | 1.439 | 7.116 | 3/2 | 1.30(11)[b] | 385(20) | 7.88 | –1.40 | |
| $^{66}$Zn | 42 | 3.898 | 53 | 4.119 | | | | | 7.50 | 0.48 | |
| $^{66}$Ga | 28 | 0.974 | 34 | 1.076 | | | | | 8.00 | –2.10 | |
| $^{66}$Ge | 4 | 2.173 | 4 | 2.173 | | | | | 7.50 | 0.55 | |
| $^{67}$Cu | 6 | 1.937 | 5 | 1.670 | | | | | 8.20 | 0.07 | |
| $^{67}$Zn | 31 | 1.875 | 26 | 1.783 | 7.278 | 0 | 4.62(55)[b] | 390(60) | 8.04 | –1.07 | |
| $^{67}$Ga | 28 | 2.282 | 28 | 2.282 | 8.420 | 0 | 2.5(2)[a] | | 8.20 | –0.55 | |
| | | | | | 11.226 | | | [460(160)] | | | 700 |
| $^{67}$Ge | 20 | 1.747 | 20 | 1.747 | | | | | 8.05 | –0.95 | |
| $^{68}$Zn | 41 | 3.815 | 41 | 3.815 | 10.291 | 5/2 | 0.37(2)[b] | 440(60) | 8.00 | 0.60 | |
| $^{68}$Ga | 41 | 1.350 | 51 | 1.548 | 8.278 | | | [280(90)] | 8.40 | –1.70 | 304 |
| $^{68}$Ge | 16 | 3.087 | 16 | 3.087 | 12.392 | | | [550(200)] | 8.30 | 0.72 | 605 |
| $^{69}$Zn | 26 | 1.983 | 26 | 1.983 | 6.665 | 0 | 5.56(43)[b] | 320(40) | 8.75 | –0.63 | |
| $^{69}$Ga | 22 | 2.251 | 22 | 2.251 | 10.313 | | | [400(100)] | 8.75 | –0.22 | 385 |
| $^{70}$Zn | 21 | 3.246 | 21 | 3.246 | | | | | 8.50 | 0.72 | |
| $^{70}$Ga | 31 | 1.372 | 38 | 1.534 | 7.654 | 3/2 | 0.316(41)[b] | 266(20) | 9.00 | –1.27 | |
| $^{71}$Ga | 22 | 2.082 | 22 | 2.082 | 9.300 | | | [330(100)] | 9.10 | –0.30 | 250 |

[a]Reference [10].
[b]Reference [13].

support eventually an unusual behavior of certain excitation functions. Actually the latter results are very close to the evaluated data within the TENDL-2014 library [16], except the larger number of incident energies taken into account hereafter for the excitation functions just above reaction thresholds.

*The nuclear level densities* BSFG parameters used in the following model calculations as well as the independent data that have been involved in their setting up are given in Table I, following the low-lying levels numbers and excitation energies [12] used in the SM calculations (the second and third columns).

*The neutron optical potential* of Koning and Delaroche [18] was obviously the first option. However, we paid the due attention to the authors' remark that their global potential does not reproduce the minimum around the neutron energy of 1–2 MeV for the neutron total cross sections of the $A \sim 60$ nuclei. Following also their comment on the constant geometry parameters which may be responsible for this aspect, we applied the SPRT method [19] for determination of these parameters at energies below $\sim 20$ MeV, through analysis of the $s$- and $p$-wave neutron strength functions, the potential scattering radius $R'$, and the energy dependence of neutron total cross section $\sigma_T(E)$. The RIPL-3 recommendations [13] for the neutron resonance data and the available measured $\sigma_T$ data (Fig. 1) have been used in this respect. Thus we found it

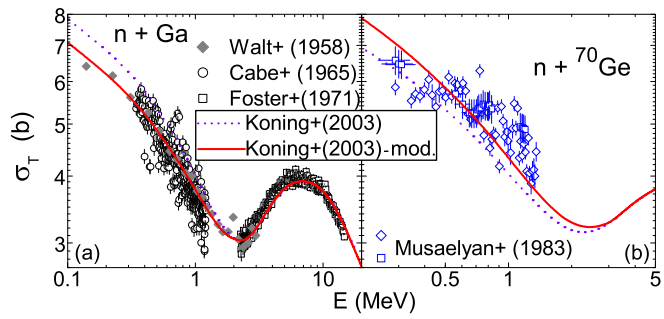


FIG. 1. (Color online) Comparison of measured [11] and calculated neutron total cross sections for Ga and $^{70}$Ge, using either (a) the local $^{69}$Ga or (b) the global OMP parameters sets of Koning and Delaroche [18] (dotted curves), and additionally the energy-dependent geometry parameters mentioned in the text (solid curves).

necessary to replace the constant real potential reduced radius and diffusivity of the local parameter set for $^{69}$Ga [18], below the neutron energy of 2 MeV, by the energy-dependent forms $r_V = 1.247 - 0.015E$ and $a_V = 0.435 + 0.12E$, where the energy $E$ and parameters are in MeV and fm, respectively. These parameters were used for neutrons on Ga residual nuclei, while for neutrons on $^{67}$Ge residual nucleus we found suitable the similar change of the corresponding neutron OMP global parameters [18] by energy-dependent forms $r_V = 1.1455 + 0.02E$ and $a_V = 0.8774 - 0.07E$, below 3 MeV.

*The proton optical potential* of Koning and Delaroche [18] was also the first option for calculation of the proton transmission coefficients. Unfortunately for its validation in the case of Zn isotopes, the measured proton total reaction cross sections $\sigma_R$ for these isotopes have been available only for energies $\geqslant$10 MeV [20]. Therefore, an analysis of the $(p,n)$ reaction cross sections at the lower energies of Ref. [1] become necessary due to the well-known anomalies of proton OMP within these energies and mass range [21]. On the other hand, comparable rather accurate data and also down to the $(p,n)$ reaction effective thresholds exist only for $^{67,68}$Zn isotopes. Moreover, while the global OMP [18] provide a suitable description of data in the case of $^{68}$Zn nucleus, about 50% higher values are obtained in comparison with the even more reliable data for $^{67}$Zn (Fig. 2).

A similar overprediction was found previously for Fe and Ni isotopes [22], whereas the motivation of the difference between the two isotopes is beyond the aim of this work. Therefore, we just looked for the OMP adjustment which may lead to the data account. Thus, in order to describe the $(p,n)$ reaction cross sections for $^{67}$Zn, we found it necessary to replace the constant real potential reduced radius and diffusivity of the global parameter set [18] by the energy-dependent forms $r_V = 1.2791 - 0.005E$ and $a_V = 0.2928 + 0.025E$, below the proton energy of 15 MeV. The similar decrease of the corresponding OMP transmission coefficients provides a better agreement of the calculated and more reliable measured $(p,n)$ reaction cross sections for $^{66}$Zn (Fig. 2). Finally, the same approach was used for the cross-section calculation of the proton-induced reactions on $^{64}$Zn, while the global OMP [18] was adopted in the case of the $^{68,70}$Zn target nuclei. The data for $^{70}$Zn are again overpredicted at proton energies below ~5 MeV but well described at the higher energies where measured $(p,\alpha)$ reaction cross sections are available.

The proton OMP used in the case of the target nucleus $^{64}$Zn was also involved in calculation of the collective inelastic scattering cross sections by means of the direct interaction (DI) distorted-wave Born approximation (DWBA) method and a local version of the computer code DWUCK4 [23], by using the deformation parameters [24,25] of the first $2^+$ and $3^-$ collective states of $^{64}$Zn. Typical DI inelastic-scattering cross sections, taken into account for the $\sigma_R$ decrease within the PE+CN calculations, grow up to ~6% of $\sigma_R$ for proton energies above 10 MeV. Similar ratios of these cross sections have been used for all Zn isotopes.

*The $\alpha$-particle optical potential* for nuclei within the mass number range $45 \leqslant A \leqslant 209$ [3] has been used for both $\alpha$-induced reaction and $\alpha$-emission cross-section calculations.

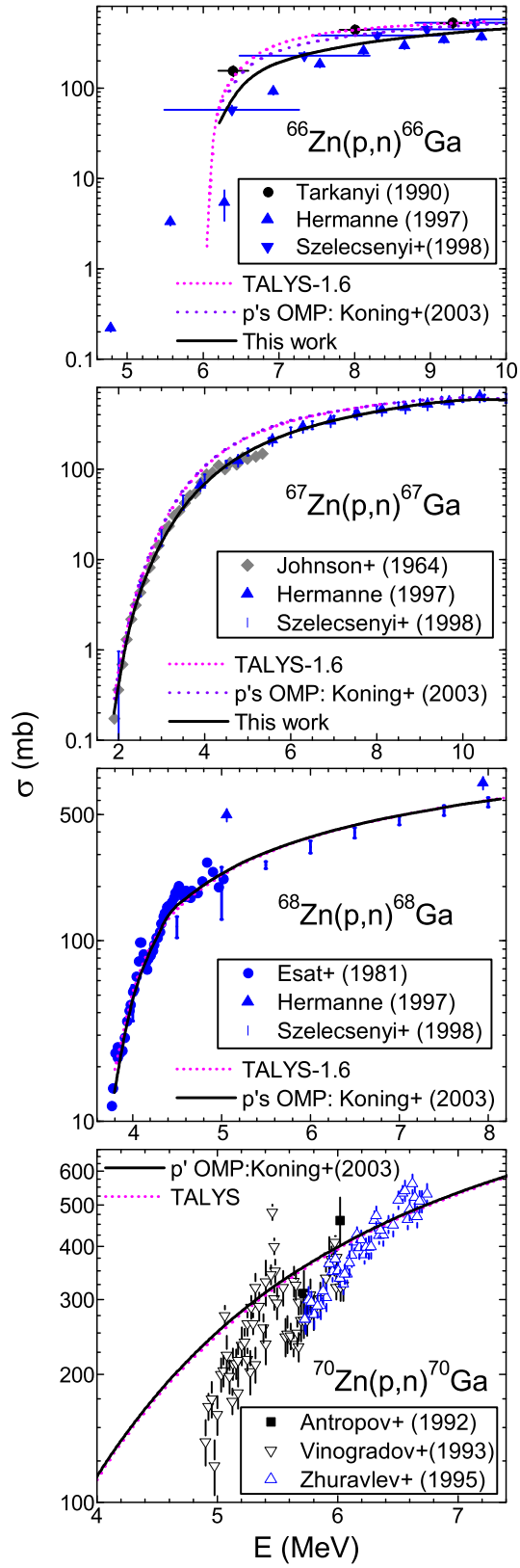


FIG. 2. (Color online) Comparison of the measured [11], global predictions of the code TALYS [15] (short-dotted curves), and calculated $(p,n)$ reaction cross sections for the $^{66,67,68,70}$Zn target nuclei using either the global OMP [18] (dotted curves) or finally adopted parameters (solid curves).

The same OMP was also involved in DWBA calculation of the cross sections for the collective inelastic scattering on $^{64}$Zn, using the above-mentioned deformation parameters [24,25] of the first $2^+$ and $3^-$ collective states of $^{64}$Zn. The collective form of the Coulomb excitation (CE) has also been considered within this approach in the usual way [23], while the comments on CE effects given in Sec. II A of Ref. [3] apply here as well. Typical DI inelastic-scattering cross sections, taken into account for the decrease of the $\alpha$-particle $\sigma_R$ within the CN calculations, grow up from ~11% to ~18% of $\sigma_R$ for $\alpha$-particle energies from 6.6 to 8 MeV, and then decrease to ~4% at the energy of ~13 MeV.

*The $\gamma$-ray strength functions* have not been established by a renormalization carried out in order to achieve agreement with the $(\alpha,\gamma)$ data (e.g., Ref. [26]), but on the basis of the radiative strength function (RSF) measured data. Unfortunately, unlike a previous opportunity [3] to use high-accuracy RSF measurements at lower energies of the corresponding excited nuclei [27,28], only former RSF data for neighboring nuclei $^{61,62,63,64,65}$Cu, $^{64,66}$Zn, and $^{69}$Ga [29–34] have been available for the present analysis.

The former Lorentzian (SLO) [35], the generalized Lorentzian (GLO) [36], and the enhanced generalized Lorentzian (EGLO) [37] models have been used for the electric-dipole $\gamma$-ray strength functions, of main importance for calculation of the $\gamma$-ray transmission coefficients. The giant dipole resonance (GDR) line-shape usual parameters derived from photoabsorption data for Ga [38] and $^{70}$Ge [39] nuclei were used in this respect. Since there are no measured $s$-wave average radiation widths $\Gamma_\gamma$ to be used for fixing the EGLO parameters [37], we have looked for a suitable description of the RSF data for the above-mentioned neighboring nuclei (Fig. 3). This aim has been achieved using the EGLO model with a constant nuclear temperature $T_f$ of the final states [40], while the SLO model was used for the M1 radiation, with the global parametrization [13] for the GDR energy and width, i.e., $E_0 = 41A^{1/3}$ MeV and $\Gamma_0 = 4$ MeV, but a value of 1 mb for its peak cross section. The latest parameter value is not related to the systematics of $f_{M1}(E_\gamma = 7\,\mathrm{MeV}) = 1.58 \times 10^{-9} A^{0.47\pm0.21}$ [41] since most of the excited nuclei within present work have neutron binding energies much different from a value of 6–7 MeV. Finally, we found that a value $T_f = 0.5$ MeV led to the agreement of the RSF data and the sum of the RSF of E1 and M1 radiations (Fig. 3), this sum being actually rather close to the former term.

The calculated $\Gamma_\gamma$ values corresponding to the adopted $\gamma$-ray strength functions are also given in Fig. 3 for each E1 model involved in the present work. They are compared to the values deduced from systematics of the measured-data dependence on the neutron separation energy $S$. While a recent similar analysis for the $^{76}$Ge nucleus used a linear fit in this respect for all Ge isotopes [42], the related $S$ value being in between the other ones, the much larger $S$ values for the excited $^{65}$Ga and $^{68}$Ge nuclei led us to the use of the quadratic dependence previously involved also by the Oslo group [43]. Thus, on the basis of the $\Gamma_\gamma$ data available for the nuclei with the atomic number $Z = 31$–$38$ [13] except the neutron-closed shell, rather rough estimations have been obtained (Table I). In spite of the low accuracy of these estimations for the $^{65}$Ga and $^{68}$Ge

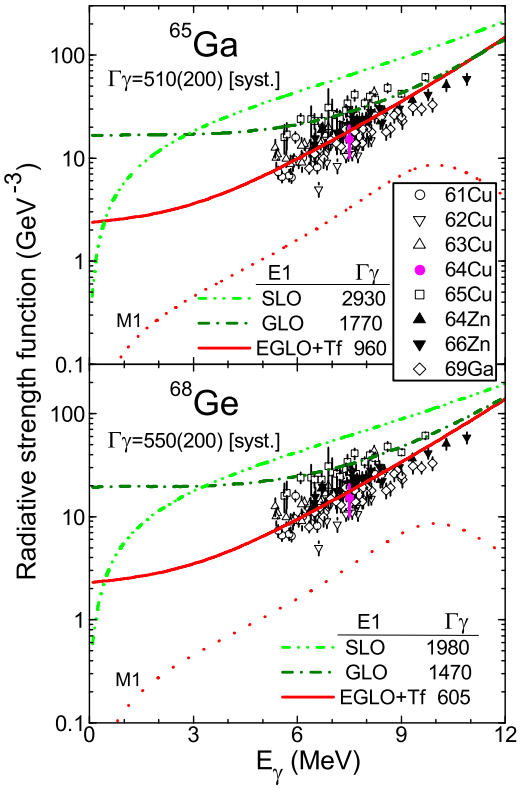


FIG. 3. (Color online) Comparison of calculated $\gamma$-ray strength functions of the $E1$ and $M1$ radiations for the $^{65}$Ga and $^{68}$Ge nuclei, using to the SLO (dash-dot-dotted curves), GLO (dash-dotted curves), and EGLO (solid curves) models for E1 radiations, and SLO model for M1 radiations (dotted curves), as well as of the calculated $s$-wave average radiation widths $\Gamma_\gamma$ (in meV) corresponding to the SLO model M1 function and each of the above-mentioned E1 model functions. There are also shown the measured dipole $\gamma$-ray strength functions for the $^{61,62,63,64,65}$Cu, $^{64,66}$Zn, and $^{69}$Ga nuclei [29–34], and the $\Gamma_\gamma$ values deduced for the two nuclei from systematics of the measured data [13].

nuclei, it results that only the EGLO $\gamma$-ray strength functions may provide values closer to them (Fig. 3). Moreover, only the same functions show a rather constant nonzero limit which is comparable to the recent RSF data obtained for $^{74,76}$Ge nuclei [42].

$(p,\gamma)$ *reaction data analysis* for the Zn target nuclei (Fig. 4) has additionally been used to check the accuracy of the adopted RSFs. The new data of Gyürky *et al.* [1] have completed a set of rather recent and precise cross sections measured across ~7 MeV above this reaction threshold, over four orders of magnitude. A large body of rather precise earlier data but across a smaller energy range there is only for the $^{68}$Zn isotope. Both of them are well described by the parameters adopted in the present work, with a distinct difference of even a factor >2 for the excitation-function maxima if the EGLO model is replaced by the GLO one. An additional similar factor is given by the use of the SLO model.

The data of the $^{64}$Zn isotope have the additional advantage to be free of any neutron-emission competition, contrary to the case of $^{68}$Zn. At the same time, it is obvious the additional change of the calculated cross sections for $^{64}$Zn due to the use

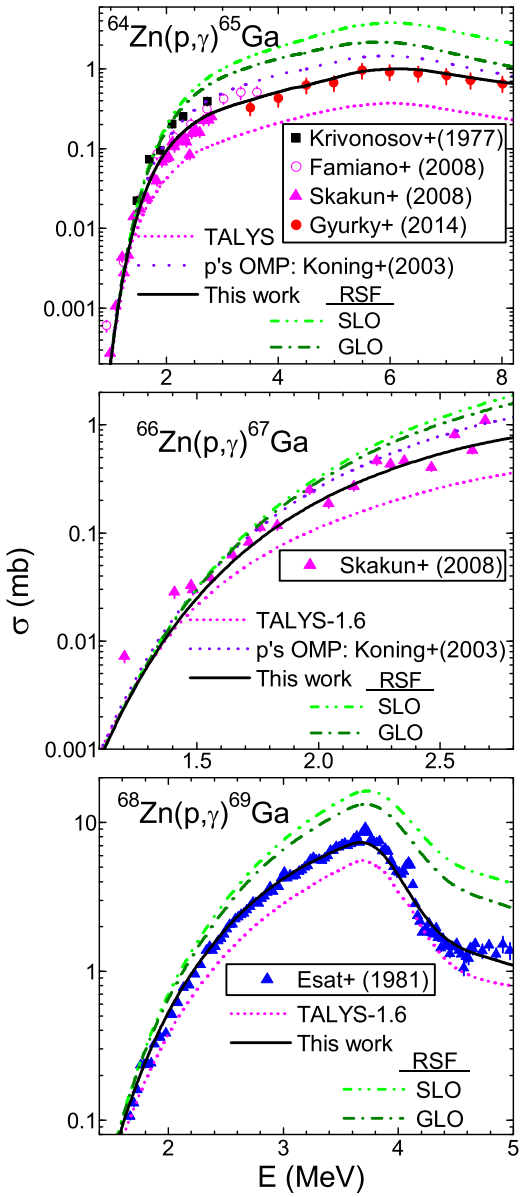


FIG. 4. (Color online) Comparison of the measured [1, 11], global predictions of the code TALYS [15] (short-dotted curves), and calculated cross sections for the $(p,\gamma)$ reaction on $^{64,66,68}$Zn using the proton OMPs and EGLO-model RSFs given in the text, with alternate involvement of either the global OMP [18] (dotted curves) or different RSFs, namely the GLO- (dash-dotted curves) or SLO-model (dash-dot-dotted curves) RSFs.

of the proton global OMP [18]. However, this latter change is about half of that related to the adopted RSF model. On the other hand, one may note that the agreement between the calculated and measured cross sections for each of the two isotopes $^{64,68}$Zn provides, beyond the RSF approach, additional support for distinct types of adopted SM parameters, namely the proton and neutron OMPs, respectively. Thus results once more the usefulness of the SM parameter validation by means of various independent data.

For the sake of completeness, we show also the results for only one available set of more recently measured $(p,\gamma)$ reaction cross sections for the $^{66}$Zn isotope, over just ∼2 MeV above the threshold, where there is again no competition of the neutron emission. The spread of these data is too large in order to get a definite estimation of the calculated values. Actually this spread is comparable to the changes that may appear by using the proton global OMP [18]. Nevertheless, it is obvious that only the EGLO $\gamma$-ray strength function may describe also these data in spite of a minor underestimation that is much larger for the TALYS predictions.

## III. RESULTS AND DISCUSSION

### A. $(\alpha,x)$ reaction data analysis

A worthy description of the $(\alpha,\gamma)$, $(\alpha,n)$, and $(\alpha,p)$ reaction data altogether, for energies $\leqslant B$ in the mass range $A \sim 60$, was given earlier [7] only for $^{58,62}$Ni (also confirmed by new measurements [44]). Therefore, the analysis of the new set of high precision data for the three reactions on $^{64}$Zn [9] is particularly worthwhile.

The agreement of the new measured data [9] and the calculated results using the $\alpha$-particle OMP [3] is rather good particularly for the $(\alpha,p)$ and $(\alpha,n)$ reaction cross sections (Fig. 5). This is most important especially in the energy ranges where each of these reactions accounts for the largest fraction of the total reaction cross section. This is the case of the $(\alpha,p)$ reaction at incident energies above ∼8 MeV and before the $(\alpha,n)$ reaction threshold, while the latter reaction is then dominant. The $\alpha$-particle OMP is thus well supported. A slight difference there is between the measured and calculated $(\alpha,p)$ reaction cross sections just above the threshold but in the limit of the data error bars. There is some underestimation of one $(\alpha,n)$ data point measured just above the threshold, which is even larger for either the TALYS prediction or potential of McFadden and Satchler [5].

Concerning the latter $\alpha$-particle OMP [5], which definitely works very well for a potential having only four constant parameters and no surface imaginary component, a further note should concern the slope of the corresponding $(\alpha,p)$ excitation function. It is lower than the experimental one and the results provided by the former OMP [3], the related cross sections being larger by more than 60% at the lowest incident energies while they are ∼20% lower above 10 MeV. Thus, a crossover appears for the two calculated excitation functions at the incident energy of about 8 MeV. This point, corresponding to about $0.7B$, is evident also for the $(\alpha,\gamma)$ reactions but not in the case of the $(\alpha,n)$ reaction which has a higher threshold. This is why the $(\alpha,n)$ calculated cross sections given by the McFadden and Satchler OMP above the incident energy of 10 MeV are only 10–15% lower than the measured data [9] and the results of our potential [3].

On the other hand, the accuracy of the calculated $(\alpha,n)$ reaction cross sections is not much worse due to the use of a global OMP for $\alpha$-particle [5] but for neutrons [18] (bottom of Fig. 5). The Koning-Delaroche potential was actually established over 200 MeV and thus it is obviously less accurate within a small energy range around 1 MeV.

The present calculated results somewhat underestimate the $^{64}$Zn$(\alpha,\gamma)^{68}$Ge reaction cross sections measured at few

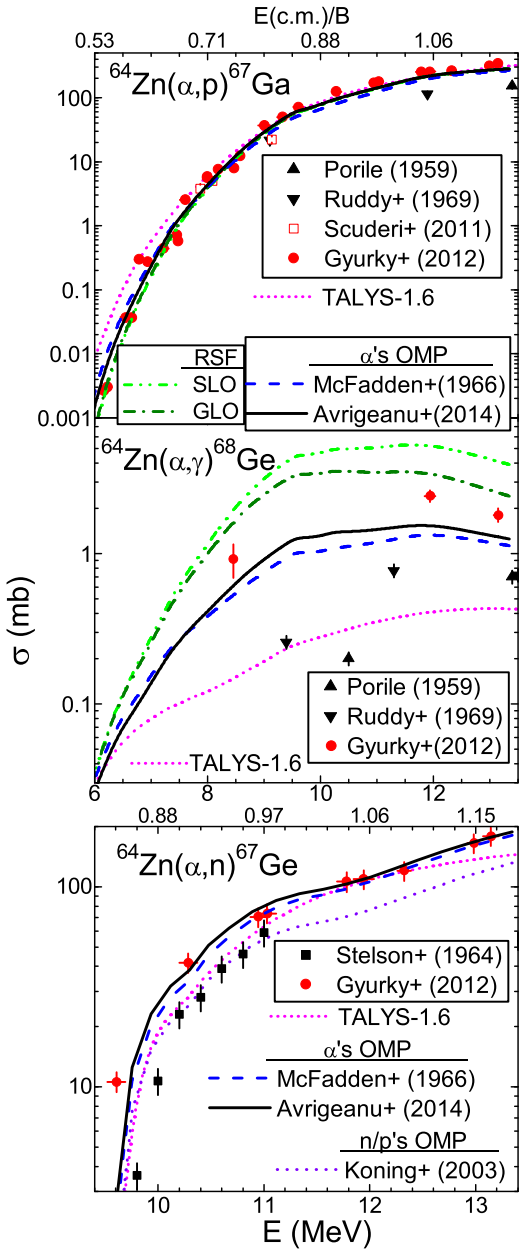


FIG. 5. (Color online) As Fig. 4 but for the $\alpha$-induced reactions on $^{64}$Zn [9,11], calculated using the $\alpha$-particle global OMPs of either Ref. [5] (dashed curves) or Ref. [3] (solid curves), and the alternate involvements done in the case of the latter $\alpha$-particle OMP.

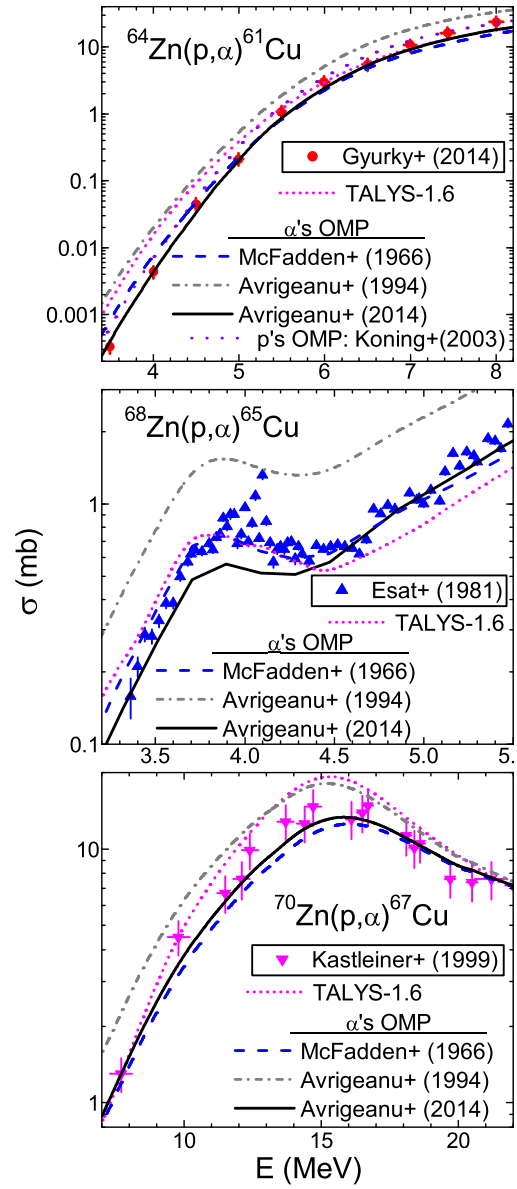


FIG. 6. (Color online) As Fig. 5 but for the $(p,\alpha)$ reaction on $^{64,68,70}$Zn, and the alternate use of the $\alpha$-particle OMP of Ref. [2] (short dash-dotted curves).

energies by the activation method which is however not optimal in this case [9]. However, the results obtained with the McFadden and Satchler potential [5] and especially the TALYS predictions are even less suitable. On the other hand, the use of the above-mentioned RSFs shows that, while the EGLO model led to underestimation of the measured data, the GLO one overestimated them. Therefore, the support of the former RSF model by the corresponding data (Fig. 3) has been the decisive factor to use the EGLO model in spite of the less suitable account of the $(\alpha,\gamma)$ data. Nevertheless, only further cross-section measurements already planned [9] within a different method, or more appropriate RSF data, could make clear this point.

### B. $(p,\alpha)$ reaction data analysis

The analysis of the available $(p,\alpha)$ reaction data for all Zn stable isotopes is an ultimate check of the emitted $\alpha$-particle OMP, once the nucleon OMPs and RSF were fixed by analysis of independent measured data, and confirmed through SM cross-section calculations mostly sensitive to each of them.

First, a suitable description of the $^{64}$Zn$(p,\alpha)^{61}$Cu reaction cross sections [1] over five orders of magnitude (Fig. 6) has been obtained in the limit of error bars by using the global OMP for incident $\alpha$ particles [3]. At the same time, a comparison of the results provided by this potential and that of McFadden and

Satchler [5] shows that the latter are ∼25% lower above 8 MeV but more than twice larger at the lowest incident energies. On the other hand, even larger overestimation of the $(p,\alpha)$ reaction data in the energy range of Ref. [1] is given by the OMP established for $\alpha$ emission in the early 1990s [2] by extrapolation to the low energies of a potential based on the $\alpha$-particle elastic scattering at high energies.

A significant common point of the two OMPs [2,5] which overestimate these $(p,\alpha)$ data is the rather similar slope but lower than the experimental data trend. This may suggest that the common lack of the surface imaginary component of these potentials, with the specific energy dependence discussed in Refs. [3,8], leads to the improper description of the measured energy dependence of the $\alpha$-particle emission.

One may also note that the use of the proton global OMP [18] led to a significant change of the calculated cross sections in the whole incident-energy range which is close to that given by the use of the $\alpha$-particle OMP of McFadden and Satchler at lowest energies. Therefore, a usual global model calculation may provide twice larger variation of the calculated data at these energies, around actually the similar TALYS results that were considered in Ref. [1].

Second, the analysis of the earlier data available for the $^{68}$Zn target nucleus may validate our potential [3] also for the $\alpha$ emission, provided that one pays more attention to the incident energies which are either lower or higher than the isobaric analog resonances (IAR) around the proton energy of 4.1 MeV [45]. On the contrary, the results corresponding to the OMP of McFadden and Satchler [5] go through the IAR data region but are higher and lower than the rest of data at the lower or higher energies, respectively. Therefore, comparison of measured and calculated $\alpha$-emission data for this target nucleus, which has been considered here first to proof the $\alpha$-particle OMP for all isotopes of Zn, has pointed out also the usefulness of the actual high-precision measurements [1] for much lower incident energies and reaction cross-section values.

Third, the available data extension above the upper end of the energy range of Ref. [1], for the $^{70}$Zn target nucleus, made possible a check of the concerned $\alpha$-particle OMP at higher energies, including the $\alpha$-particle PE. The PE calculation within the present work has made use of the same assumptions and parameters given earlier for nucleon-induced reactions in this mass region [22]. The calculated $(p,\alpha)$ reaction cross sections show a good agreement with the measured data at the low energy of ∼8 MeV, with no significant PE contribution, as well as at higher energies (bottom of Fig. 6). Actually, there are no major PE effects even at proton energies around 20 MeV. Thus, while the PE fraction goes from below 1% to above 4% of $\sigma_R$, for the proton energies below ∼8 MeV on $^{64,70}$Zn, respectively, it becomes larger than 20% only above 20 MeV. On the other hand, the importance of the $(p,\alpha)$ reaction data of $^{70}$Zn is related to the emission of $\alpha$ particles with energies also above ∼ 10 MeV, as mentioned below.

The basic point of the $\alpha$-particle OMP of Refs. [3,7,8] is related to the $\alpha$-particle nuclear surface absorption with an energy-dependence major change at an $\alpha$-particle energy $E_2$ corresponding to $0.9B$. Thus, first the surface imaginary potential depth is either constant for $\alpha$-particle energies lower than a value $E_1$, or increases with the energy increase between $E_1$ and $E_2$, as more and more channels are thus opened, while it decreases above $E_2$ and eventually vanishes at the same time with the volume component becoming larger and larger. Since the elastic-scattering analysis is performed at energies above $B$, it facilitates the description of the latter side of the surface imaginary-potential energy dependence. Thus, the extrapolation to lower energies of this partial trend becomes unphysical, so that only the analysis of $\alpha$-induced reactions can provide a sound understanding of the $\alpha$-particle OMP below $B$. The point is that the energy limit $E_2$ has just the value ∼10 MeV for the $\alpha$-induced reactions on $^{64}$Zn [9] and $\alpha$-emission data of Ref. [1]. Therefore, the suitable description of these these data provides a powerful support for the $\alpha$-particle OMP [3] just below and around $B$. Subsequently, this support is extended to the energy range of elastic-scattering data by the agreement obtained for the $(p,\alpha)$ reaction on $^{70}$Zn at incident energies corresponding to emitted $\alpha$-particle energies also beyond the $E_2$ value.

## IV. CONCLUSIONS

Recent accurate $(p,\alpha)$ reaction data for the target nucleus $^{64}$Zn [1] have been analyzed simultaneously with similar data for the competitive $\gamma$ rays and the available data for proton-induced reactions on the other Zn isotopes. The $\alpha$-induced reactions on the same $^{64}$Zn nucleus have similarly been considered. The $\alpha$-particle energies corresponding to each of these reactions were either below or around the Coulomb barrier. While the description of both $\gamma$-ray and $\alpha$-particle emission were found problematic within the above-mentioned study of protons on $^{64}$Zn [1], a careful assessment of the related quantities was first undertaken in the present work. This goal was achieved through various independent data analysis. Thus, the transmission coefficients of protons and $\gamma$ rays, given by the corresponding optical potential and $\gamma$-ray strength functions, respectively, have been fixed by independent analysis of $(p,n)$ reaction and radiative strength functions data. Then, they have also been checked by means of $(p,\gamma)$ reaction data. As a result, the accurate $(p,\alpha)$ reaction data became indeed uniquely sensitive to the $\alpha$-particle optical potential. Evidence for the correctness of the $\alpha$-particle global optical potential [3] within both incident and outgoing channels has been thus found. Additionally, this potential has been supported by the suitable description of recent data for $\alpha$-induced reactions on $^{64}$Zn nucleus, using the same above-mentioned consistent set of input parameters.

There have been several critical features of the statistical model parameters which led to particular conclusions of the present work. Thus, a quite reliable set of $(p,n)$ reaction cross sections for $^{67}$Zn pointed out the need to use energy-dependent geometry parameters below the proton energy of 15 MeV, together with the rest of widely used OMP parameters of Koning and Delaroche [18]. The same parameters provide also a rather good account of more reliable measured $(p,n)$ reaction cross sections for $^{66}$Zn, while their use for the target nucleus $^{64}$Zn results in about 50% lower calculated cross sections of the $(p,n)$ reaction. On the other hand, an independent setting up of the $\gamma$-ray strength functions was carried out on the basis of

available measured data which have been, unfortunately, neither recent nor for lower energies of the corresponding excited nuclei. Nevertheless, the additional analysis of the available $(p,\gamma)$ reaction data on Zn isotopes has eventually validated both the adopted proton OMP and $\gamma$-ray strength functions.

Concerning the well-known $\alpha$-particle global potential of McFadden and Satchler [5], it provides calculation results which exceed the data by more than a factor $\geqslant 2$ at the lowest proton incident energies of Ref. [1] while they are $\sim$25% lower above 8 MeV. The corresponding overestimation of the lowest-energy $(p,\alpha)$ reaction data [1] is increased by the use of the proton global optical potential [18], leading to the TALYS results that were considered too in Ref. [1]. Therefore the $(p,\alpha)$ reaction analysis is a powerful approach for the $\alpha$-particle optical potential analysis, provided that the proton optical potential is additionally validated by means of independent data. On the other hand, the progress of the $\alpha$-particle global [3], which provides a suitable description of the $\alpha$-particle induced reaction data within the wide mass range $45 \leqslant A \leqslant 209$, should be validated for $\alpha$-particle emission over the same $A$ range.

## ACKNOWLEDGMENT

This work was partly supported by Fusion for Energy (F4E-GRT-168-02), and by Autoritatea Nationala pentru Cercetare Stiintifica (PN-09370105).

[1] Gy. Gyürky, Zs. Fülöp, Z. Halász, G. G. Kiss, and T. Szücs, Phys. Rev. C **90**, 052801(R) (2014).
[2] V. Avrigeanu, P. E. Hodgson, and M. Avrigeanu, Phys. Rev. C **49**, 2136 (1994).
[3] V. Avrigeanu, M. Avrigeanu, and C. Mănăilescu, Phys. Rev. C **90**, 044612 (2014).
[4] M. Avrigeanu, W. von Oertzen, and V. Avrigeanu, Nucl. Phys. A **764**, 246 (2006).
[5] L. McFadden and G. R. Satchler, Nucl. Phys. A **84**, 177 (1966).
[6] M. Avrigeanu, W. von Oertzen, A. J. M. Plompen, and V. Avrigeanu, Nucl. Phys. A **723**, 104 (2003).
[7] M. Avrigeanu, A. C. Obreja, F. L. Roman, V. Avrigeanu, and W. von Oertzen, At. Data Nucl. Data Tables **95**, 501 (2009).
[8] M. Avrigeanu and V. Avrigeanu, Phys. Rev. C **82**, 014606 (2010).
[9] Gy. Gyürky, P. Mohr, Zs. Fülöp, Z. Halász, G. G. Kiss, T. Szücs, and E. Somorjai, Phys. Rev. C **86**, 041601(R) (2012).
[10] H. Vonach, M. Uhl, B. Strohmaier, B. W. Smith, E. G. Bilpuch, and G. E. Mitchell, Phys. Rev. C **38**, 2541 (1988).
[11] Experimental Nuclear Reaction Data (EXFOR), http://www-nds.iaea.org/exfor/.
[12] Evaluated Nuclear Structure Data File (ENSDF), http://www.nndc.bnl.gov/ensdf/.
[13] R. Capote *et al.*, Nucl. Data Sheets **110**, 3107 (2009); http://www-nds.iaea.org/RIPL-3/.
[14] M. Avrigeanu and V. Avrigeanu, IPNE Report No. NP-86-1995, Bucharest, 1995, and refs. therein; News NEA Data Bank **17**, 22 (1995).
[15] A. J. Koning, S. Hilaire, and M. C. Duijvestijn, v. TALYS-1.6, 2013, http://www.talys.eu.
[16] A. J. Koning and D. Rochman, *TENDL-2014: TALYS-Based Evaluated Nuclear Data Library*, 2013, http://www.talys.eu/tendl-2014/.
[17] V. Avrigeanu, T. Glodariu, A. J. M. Plompen, and H. Weigmann, J. Nucl. Sci. Technol. Suppl. **2**, 746 (2002); http://tandem.nipne.ro/~vavrig/publications/2002/Tables/caption.html.
[18] A. J. Koning and J. P. Delaroche, Nucl. Phys. A **713**, 231 (2003).
[19] J. P. Delaroche, Ch. Lagrange, and J. Salvy, *IAEA-190* (IAEA, Vienna, 1976), Vol. 1, p. 251.
[20] R. F. Carlson, At. Data Nucl. Data Tables **63**, 93 (1996).
[21] S. Kailas, M. K. Mehta, S. K. Gupta, Y. P. Viyogi, and N. K. Ganguly, Phys. Rev. C **20**, 1272 (1979).
[22] M. Avrigeanu, S. V. Chuvaev, A. A. Filatenkov, R. A. Forrest, M. Herman, A. J. Koning, A. J. M. Plompen, F. L. Roman, and V. Avrigeanu, Nucl. Phys. A **806**, 15 (2008).
[23] P. D. Kunz, DWUCK4 user manual, OECD/NEA Data Bank, Issy-les-Moulineaux, France, 1984; www.oecd-nea.org/tools/abstract/detail/nesc9872.
[24] S. Raman, C. W. Nestor, and P. Tikkanen, At. Data Nucl. Data Tables **78**, 1 (2001).
[25] T. Kibédi and R. H. Spear, At. Data Nucl. Data Tables **80**, 35 (2002).
[26] G. G. Kiss *et al.*, Phys. Rev. C **88**, 045804 (2013).
[27] A. Schiller, L. Bergholt, M. Gutteormsen, E. Melby, J. Rekstad, and S. Siem, Nucl. Instrum. Methods Phys. Res., Sect. A **447**, 498 (2000).
[28] http://www.mn.uio.no/fysikk/english/research/about/infrastructure/OCL/nuclear-physics-research/compilation/.
[29] K. Nilson, B. Erlandsson, and A. Marcinkowski, Nucl. Phys. A **391**, 61 (1982).
[30] K. Nilson, B. Erlandsson, and A. Marcinkowski, Nucl. Phys. A **348**, 1 (1980).
[31] T. Belgya *et al.*, Technical Report No. IAEA-TECDOC-1506, IAEA, Vienna, Austria, 2006, p. 97; https://www-nds.iaea.org/RIPL-2/gamma/gamma-strength-exp.dat.
[32] B. Erlandsson, K. Nilson, A. Marcinkowski, and J. Piotrowski, Z. Physik A **293**, 43 (1979).
[33] B. Erlandsson, K. Nilson, and A. Marcinkowski, Nucl. Phys. A **343**, 197 (1980).
[34] K. Nilson, B. Erlandsson, L. Spanier, and A. Marcinkowski, Nucl. Phys. A **401**, 460 (1983).
[35] P. Axel, Phys. Rev. **126**, 671 (1962).
[36] J. Kopecky and M. Uhl, Phys. Rev. C **41**, 1941 (1990).
[37] J. Kopecky, M. Uhl, and R. E. Chrien, Phys. Rev. C **47**, 312 (1993).
[38] http://www-nds.iaea.org/RIPL-2/gamma/gdr-parameters-exp.dat.
[39] http://www-nds.iaea.org/RIPL-3/gamma/.
[40] A. C. Larsen and S. Goriely, Phys. Rev. C **82**, 014318 (2010).
[41] P. Obložinský *et al.*, Technical Report No. IAEA-TECDOC-1034, IAEA, Vienna, Austria, 1998; http://www-nds.iaea.org/ripl/.
[42] A. Spyrou *et al.*, Phys. Rev. Lett. **113**, 232502 (2014).
[43] H. K. Toft *et al.*, Phys. Rev. C **83**, 044320 (2011); A. C. Larsen *et al.*, **87**, 014319 (2013).
[44] S. J. Quinn *et al.*, Phys. Rev. C **89**, 054611 (2014).
[45] M. T. Esat, R. H. Spear, J. L. Zyskind, M. H. Shapiro, W. A. Fowler, and J. M. Davidson, Phys. Rev. C **23**, 1822 (1981).